Development of Image Stabilization System for the Kodaikanal Tower Telescope

A thesis submitted to the

Department of Applied Optics and Photonics
University of Calcutta

in partial fulfillment of the requirements
for the award of the degree of
Master of Technology
Astronomical Instrumentation

by

C. Shanti Prabha

Under the Guidance of

Dr. R. Sridharan

Declaration of Authorship

Declaration I hereby declare that the thesis entitled "Development of Image Stabilization System for Kodaikanal Tunnel Telescope" submitted to the University of Calcutta in the Department of Applied Optics and Photonics, in partial fulfilment of the requirements for the award of the degree of Master of Technology, is a result of the project work carried out by me at Indian Institute of Astrophysics, Bangalore under the supervision of Dr. R. Sridharan. The results presented herein have not been subject to scrutiny, by any university or institute, for the award of a degree, diploma or fellowship whatsoever.

Signed:

_____

Date:
Indian Institute of Astrophysics
Bangalore-560034
India

Certificate

This is to certify that the thesis entitled "Development of Image Stabilization System for the Kodaikanal Tower Telescope" submitted to University of Calcutta by Ms. C.Shanti Prabha in partial fulfillment of the requirements for the award of the degree of Master of Technology in Astronomical Instrumentation is based on the results of the project work carried out by her under our supervision and guidance, at the Indian Institute of Astrophysics. This thesis has not been submitted for the award of any degree, diploma, fellowship, etc. of any university or institute.

ABSTRACT

This M. Tech. project is a part of IIA's internal project of developing and demonstrating a solar adaptive optics system. The Earth's turbulent atmosphere distorts the light wave-fronts passing through it and thus impairs the resolution and the sensitivity of the ground-based telescopes. An image stabilization system aims to arrest the fast image motion induced by the atmosphere and thus forms the first step in any adaptive optics system. The main objective of this M. Tech. project is to design and develop an image stabilization system (ISS) for the KTT. This is achieved by introducing tilts at re-imaged pupil plane with a plane mirror mounted on a piezo-electic stage. In this report, the laboratory experimental setup of the ISS and the calibration of the piezo-electric stage are presented along with the current status and the future directions.

Acknowledgements

I would like to express my sincere thanks to Dr. R. Sridharan for his constant support and help during this project. He was available every time when I needed and helped me in every aspect of my work. I am grateful to Dr. R. Banyal, Dr. Subinoy Das and Dr. Mousumi Das for their invaluable classes. I am also thankful to faculty at University of Calcutta, namely Prof. K. Bhattachaya, Prof. A. Ghosh, Prof. L.N. Hazra, Prof. Nabajit Chakravarty, Prof. A.B. Ray, Prof. Samir Sarkar, Prof. A. Chakrabarty, Prof. R. Chakraborty, Dr. M. Ray, Dr. K.Palodhi and Dr.Sanjukta Sarkar for their wonderful teaching and support. I am grateful to BGS committee for it's continuous support. I'd like to thank the computer support team for helping me in resolving troubleshooting of systems and installing the necessary software as and when needed. I express my sincere thanks to the director, the academic and administrative staff and my fellow students of IIA for their support during the last two years.

Contents

List of Figures

List of Tables

Prologue

IIA is deliberating on building a 2m class solar telescope (named as the National Large Solar Telescope(NLST)) at Merak near the Himalayas. This telescope will be equipped with an adaptive optics facility. In preparation for such a large solar observing facility equipped with adaptive optics, it is desirable to generate the necessary expertise by demonstrating solar adaptive optics on existing small solar telescopes. IIA has initiated an internal project on solar adaptive optics to accomplish the same.

This M. Tech. project is a part of IIA's internal project of developing and demonstrating a solar adaptive optics system. The Earth's turbulent atmosphere distorts the light wave-fronts passing through it and thus impairs the resolution and the sensitivity of the ground-based telescopes. A major component of this distortion is the random tilting of the wave-front at kHz rate. This fast random wave-front tilt is manifested as random motion of the image at the focal plane of the telescope. Consequently, the image is blurred when the exposure time is larger than a few tens of milli-seconds. An image stabilization system aims to arrest the fast image motion induced by the atmosphere and thus forms the first step in any adaptive optics system.

Chapter 1

Introduction

1.1 A primer on Adaptive Optics

The Earth's atmosphere through which light from a celestial object propagates is turbulent. Temperature fluctuations in the atmosphere cause fluctuations in the refractive index and this makes different parts of the light to traverse differently. This leads to a distorted wave-front (surface of constant phase). As a result, the image formed by ground-based telescopes is blurred and the resolution is impaired.

The purpose of an adaptive optics is to actively sense and correct wave-front distortions at the telescope during observations. A telescope equipped with an adaptive optics measures wave-front distortions with a sensor and then applies phase corrections with a deformable mirror on a time scale comparable to the temporal variations of the atmospheric phase fluctuations.

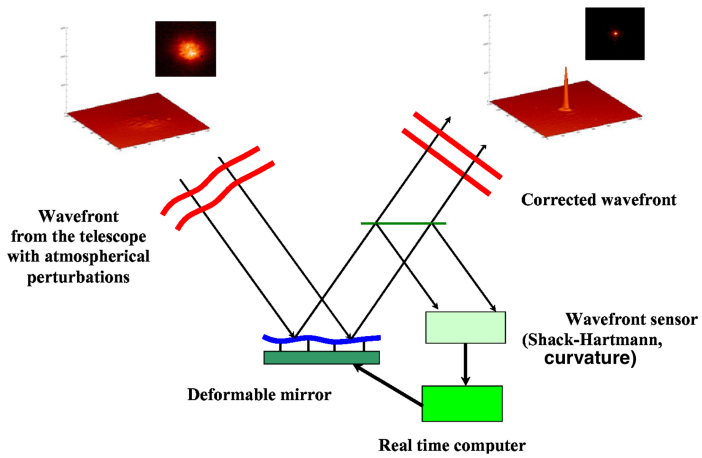

FIGURE 1.1: Pictorial representation of an AO system. Distorted wave-fronts result in poor resoluion image (top left). Corrected wave-fronts lead to better resolution (top right). Wave-front sensing, correction and control computer form the three major components of an AO system.

1.2 Parts of an AO system

1.2.1 Wavefront sensors

A wave-front sensor is used to characterize the wave-front distorted by atmospheric turbulence for real time wave front correction. In a closed loop adaptive optics system, it measures the residual phase at various points on the wave-front.

1.2.1a Shack-Hartman sensor

An array of lens-lets is used to spatially sample the wave-front and the form an array of images known as spot-fields. The shifts in the centroid of the spot-fields measured at the image plane are related to the local slopes of the wave-front over the lens-lets. Measurement noise arises from an uncertainty in the determination of centroid position of each spots. Range and accuracy of measurement depend on CCD performance and diffraction and defects of lens-let array. The global shape of the wave-front over the pupil is estimated from the local slopes.

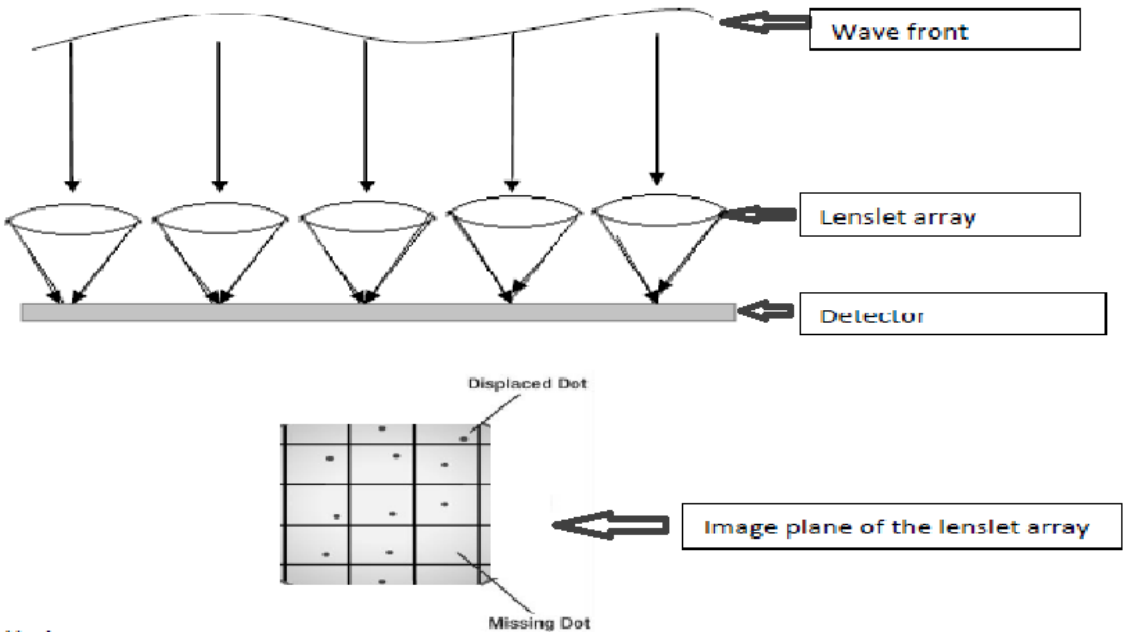

FIGURE 1.2: The Shack-Harttmann wavefront sensor-top:wavefront is entering from top, falls on a lens-let array. Images are formed at the detector placed at the focal plane of the lens-lets, bottom: A segment of the detector plane containing a few spot-fields formed by a 2D lens-let array.

1.2.1b Curvature sensor

The curvature sensor was invented by F.Roddier [Roddier and Roddier, 1988].15. Figure 1.3 indicates the principle of curvature sensing. A positive curvature creates more brightness in plane P1 and negative curvature creates more brightness in plane P2. This difference in brightness between the planes provides a measure of local curvature.

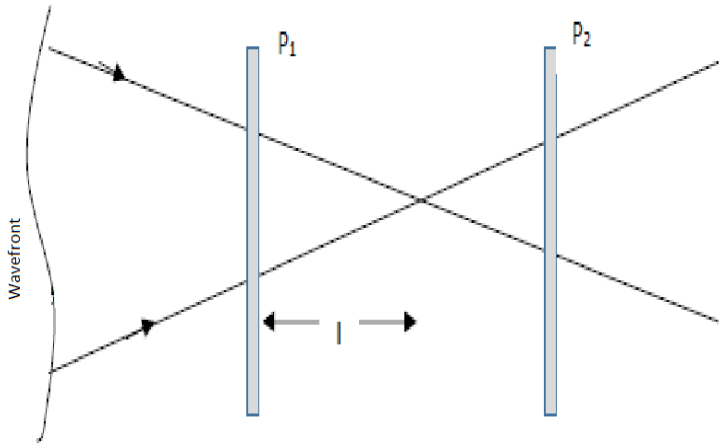

FIGURE 1.3: The Curvature wavefront sensor-the wavefront after being focused is entering from left, l is the distance of the focus point from the plane P_1, P_1 and P_2 are the planes where the intensities are measured.

1.2.2 Wavefront correctors

Wave-front correctors are basically mirrors whose surface can be deformed by attaching an actuators at their backside. The mirror may either be rigid and segmented or a thin continuous sheet. When it is rigid, a single mirror segment can correct for local piston and tip-tilt. For big telescopes many such segments may be used. When it is a thin continuous sheet, the actuators act together to produce the desired wave-front surface. Membrane mirrors or Bimorph mirrors fall in this category.

The actuators work based on piezo-electic effect, magneto electric effect or elecrostatic effect (in micro-opto-electromechanical systems). They receive their input signals through a control computer that generates the desired signals based on wave-front sensing data and a suitable control software (e.g. PID).

1.2.3 Computer

A fast real time computer is required to process the wave-front sensor data and generate the correction signals that are to be sent to the wave-front corrector actuators following certain control algorithms. The processing of the wave-front sensor data can be achieved either through hardware (FGPA, DSP boards) or software.

Software Programming: A computer software carries out the instructions of a sequential program (which would be written previously), performing low level operations (arithmetic, logical...) on the data made available to it through input/output operations with the help of intermediate registers, memory, and other peripherals. The time between the arrival of camera input and actuation command is higher than that for FPGA. Any changes required to be made to the program can be easily implemented.

FPGA: FPGA is a Field Programmable Gate Array. It consists of integrated circuits and as the name suggests, the devices can be programmed 'in the field'. One of the advantages of using them is higher speed of image correction 14. But it is more difficult to make changes in existing code/algorithm.

Digital Signal Processor: It is a kind of microprocessor which processes images in the form of digital signals. The time between the arrival of camera input and actuation command is higher than for FPGA.

For this project we intend to follow the software based approach.

1.3 A Brief Survey of the Existing Solar AO systems

- GREGOR solar telescope at Teide observatory, Tenerife, Spain: It has a high-order adaptive optics (AO) system with a 256-actuator deformable mirrors and a 156-subaperture Shack-Hartmann wave front sensor. The closed-loop bandwidth of is 130 Hz. The AO uses a classical Shack-Hartmann wave-front sensor. The number of sub-apertures is 156, each with an aperture of 10 cm [6].

- Big bear observatory: The low-order compensation system at the Big Bear solar observatory incorporates a piezoelectric tip-tilt mirror and the respective control electronics. The tilt range is +/-1mrad, with sub-micro radian resolution. The higher-order compensation system employs a flexible mirror with a 77.5 mm clear aperture placed in the re-imaged pupil plane. The mirror figure is controlled by 97 actuators. The AO system uses a correlating Shack-Hartmann WFS, which is sensitive to the gradient of the wave-front phase across the pupil. The wave-front phase itself is obtained by using a modal phase reconstructor. A lenslet array (f 24 mm) placed in the re-imaged pupil plane creates 76 images of the same solar surface region [7].

- MAST(Multi-Application Solar Telescope): The prototype AO system is being realized in two phases. The first phase is developing an image stabilization system to compensate the global tilt of the wave-front. The second phase consists of sensing and correcting the local tilts of the wave-front by integrating a micro-machined membrane deformable mirror with the image stabilization system and this phase is currently in progress [8].

- McMath-Pierce telescope: Telescope is used for AO observations in the infrared. The AO system has a deformable mirror with 37 actuators and a fast tip-tilt mirror controlled by a PC. The wave front sensor is a Shack-Hartmann sensor with 200 sub-apertures [9].

1.4 Jargon

In this section, we describe some of the jargon used in the field of optics and adaptive optics.

1.4.1 Point Spread Function

The Point-Spread Function (PSF) is the image of a point object as created by an optical system. The ideal PSF of a just resolved object or unresolved is a delta function. But any real optical system creates a spread of the point object. For ground-based telescopes, the PSF is the convolution of the spreads introduced by the atmosphere and that of the telescope.

1.4.2 Optical Transfer function

The Fourier transform of the point spread function is the Optical Transfer Function (OTF). The absolute value of the OTF is the Modulation Transfer Function (MTF) and the phase of the OTF is the Phase Transfer Function (PTF). Since the effects of the telescope/atmosphere are convolved with the PSF, the corresponding OTF's are multiplied. The OTF of telescope/atmosphere shows the effect of telescope/atmosphere on the image.

$$OTF_{effective} = OTF_{telescope} OTF_{atmosphere} \tag{1.1}$$

1.4.3 Strehl ratio

The Strehl ratio is the ratio of the central intensity of aberrated PSF and that of the diffraction limited PSF. Using the Marechal approximation for the variance σ^2 in the wave-front over the diameter of a telescope is:

$$S = e^{-\sigma^2} \tag{1.2}$$

This holds good only when σ^2 is small.

1.4.4 Fried parameter

The Fried parameter r_0 is a length such that for a telescope of diameter D=r0, the root mean square wavefront error over the aperture is 1 radian. It is used as a measure of how good the atmosphere seeing condition is. A higher r_0 indicates a smoother (less distorted) wavefront and a sharper PSF. In Appendix A, we demonstrate the relation between r_0 and the wave-front distortion/PSF through simulations.

1.4.5 Turbulence

The Earth's atmosphere is turbulent, as opposed to laminar. In laminar flow, non-crossing streamlines can be drawn for the flow, which is not the case for a turbulent flow. In turbulent flow, energy is dissipated from large vortices (which are approximately of the size of the container-infinity in case of atmosphere-called the Kolmogorov outer scale) to smaller and smaller vortices. In the smallest vortices (their size is called Kolmogorov inner scale of turbulence), energy is converted to heat through viscous dissipation.

1.4.6 Kolmogorov Model of Turbulence (5/3rd law)

In the equations/expressions for the structure function of the atmosphere, residual wave-front phase error etc. we come across 5/3 power. It is related to the Kolmogorov's 5/3rd law, which can be derived through dimensional analysis. Let k be the wavenumber. It is loosely associated with vortices of size k^{-1} and let l be the scale of the large eddies. l is the outer scale of turbulence. The 5/3rd law explains how the energy spectrum behaves in the inertial subrange. The energy spectrum E (in units of m^3/s^2) is related to the wave number k (m^{-1}) and rate of energy dissipation ϵ (m^2/s^3) by:

$$E \propto k^{-5/3}\epsilon^{2/3} \tag{1.3}$$

The law holds good only in the inertial range of k, where the length dimension is greater than microscale and smaller than macroscale.

1.4.7 Kolmogorov Power Spectrum

The power spectrum of the phase fluctuations $\Phi(k)$ corresponding to the path-length fluctuations induced by the atmosphere can be expressed in terms of r_0 under Kolmogorov turbulence as

$$\Phi(k) = 0.023 r_0^{-5/3} k^{-11/3} \tag{1.4}$$

Here k is the coordinate of spatial frequency and r_0 is the Fried parameter.

The phase distortions are related to the power spectrum as:

$$\phi(x, y) = \mathcal{F}(\sqrt{\Phi(k)}\, \exp(jp) \tag{1.5}$$

where $\mathcal{F}$ is the Fourier transform operator and p is a random number uniformly distributed between $\pm\pi$. This equation is used to simulate atmospherically induced phase distortions, known as phase-screens, over a region of space. More details are presented in Appendix A.

1.4.8 Seeing

Atmospheric seeing refers to image blurring caused by random phase distortion of the wavefronts entering a telescope. The image formed by a telescope has a full width half maximum(x) as

$$x = 0.98\lambda / r_0 \tag{1.6}$$

In a small telescope($D << r_0$), the image is nearly diffraction limited and has a full-width half maximum (x) of

$$x = 1.22\lambda / D \tag{1.7}$$

where λ is the wavelength of observation.

1.4.9 Speckles

Different regions of a wavefront, have different values of phase at any instant of time. The values of phase change over space and time depending on the condition of the atmosphere. Consequently, the short exposure image of a point object (star) is recorded at the focal plane of a large ground-based telescope, exhibits a cloud consisting of several tiny bright spots knowns as the speckles. These spots correspond to the regions of constructive interference. An example of speckle pattern is shown in 1.4

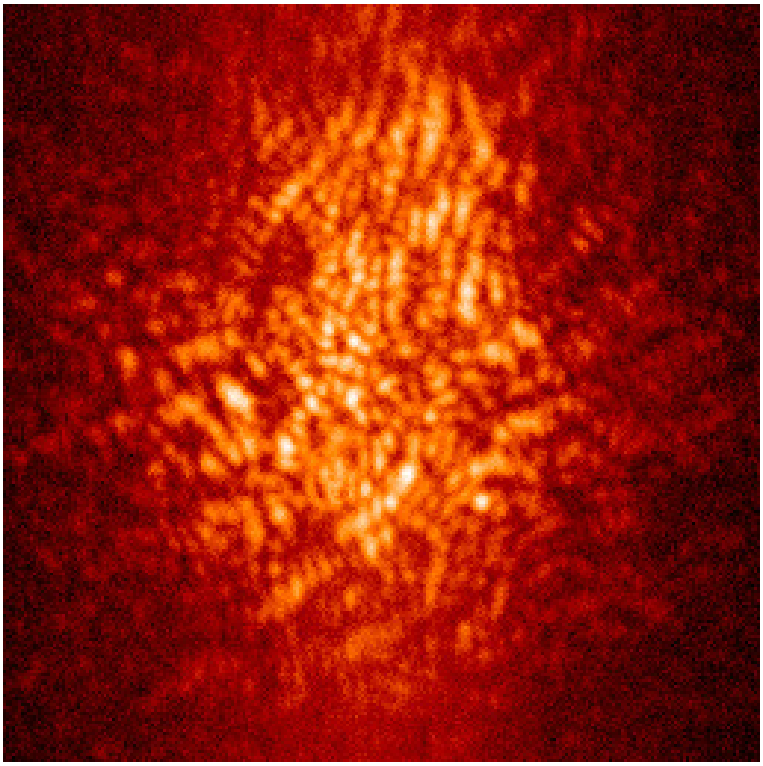

FIGURE 1.4: Short exposure (40 ms) image of a red super giant star (α Ori) recorded by the 2.34m telescope of the Vainu Bappu Observatory, Kavalur, India. The image has been presented in log scale with pseudo color.

1.4.10 Scintillation

If the wave-front is distorted, both the amplitude and the phase of the wave-front vary as a function of position on the wave-front. These amplitude fluctuations grow with distance, even

when the light propagates through regions that have no turbulence. As the turbulent cells are carried with the wind, the intensity seen by a fixed observer on the ground will vary with time. This is called scintillation. A characteristic timescale for these variations is $\tau \sim r_0/v$ where $v$is the characteristic wind velocity.

1.4.11 Atmospheric coherence time

$$\tau_0 = 0.31 r_0/v \tag{1.8}$$

where v is the wind velocity averaged over the altitude. τ_0 is a measure of how fast the AO system needs to correct the wavefront.

1.4.12 Isoplanatic angle

The angular region on the image over which the effect of atmospherically induced aberrations are the same is called the isoplanatic patch and the angular radius is called the Isoplanatic angle. The Isoplanatic angle is a measure of how spatially correlated the atmospheric phase distortion is for different object field angle. For objects lying within an isoplanatic angle, the distortions are highly correlated.

1.4.13 Iso-kinetic angle

The angle of the sky over which the motions of the objects are correlated. In a tip-tilt AO system, target stars need to lie within an Iso-kinetic angle of the guide star for the correction to be effective for both of them.

1.4.14 Phase structure function

The phase structure function is defined as the mean square variation in the phase of a wavefront.

$$D_\phi(r) = < |\phi(x) - \phi(x+r)|^2 > \tag{1.9}$$

Similarly the refractive index structure function D_n, and temperature structure function D_t are also defined as the mean square

variation in the refractive index/temperature. These structure functions are related to the distances over which they are measured by the following empirical relations:

$$D_t = C_t^2 r^{2/3} \tag{1.10}$$

$$D_n = C_n^2 r^{5/3} \tag{1.11}$$

where C_t, and C_n are the temperature, phase and refractive index structure constants respectively.

$$r_0^{-5/3} = 0.423k^2 \int C_n^2(h)dh \tag{1.12}$$

According to Kolmogorov turbulence,

$$D_\phi(r) = 6.88(\frac{r}{r_0})^{5/3} \tag{1.13}$$

The mean variance continuously increases with increasing distance according to Kolmogorov's model. For three simulated phase screens, the phase structure function was calculated using eq.1.9 and verified with theoretical eq.1.13 and the results shown in Appendix B

1.4.15 Greenwood frequency

The Greenwood frequency is the frequency or the bandwidth required for optimal correction with an adaptive optics system. It depends on the transverse wind speed and the turbulence strength in the atmosphere. It has been shown that the residual phase variance arising from the limited bandwidth of a servo system is approximated as:

$$\langle \sigma_{\mathrm{BW}}^2 \rangle = (\tau_0 f_{3\mathrm{dB}})^{-5/3}, \tag{1.14}$$

where τ_0 is the atmospheric time constant. This is true for a servo system with pure integrator. The inverse of τ_0 is called Greenwood frequency.

1.5 Zernike Representation

The ray of light entering the atmosphere is an electromagnetic wave. It can be represented by either the electric field vector or the magnetic field vector. Usually it is represented by the electric field vector whose amplitude is $Ae^{i\phi}$. Thus the wave is defined by two parameters: A, amplitude and ϕ, phase. Surfaces of a constant phase are called wavefronts.

Errors in the phase of the wave incoming from celestial objects lead to loss of clarity and degradation of the image. Errors of phase are created due to difference in the path length traveled by different rays.

Zernike showed that deviations of a wavefront from a plane wavefront can be expressed as a polynomial series and described an infinite series of polynomials named after him.

$$\phi = \Sigma_{i=0}^{\infty} a_i Z_i \tag{1.15}$$

Each polynomial can be written as $Z_n^m(\rho, \theta)$ where ρ is the radius and θ is the angle. Here n is called the radial order (based on the power of ρ occuring in the generating function of the Zernike series), and m is the azimuthal order. They can also be represented with single index(Noll's notation) as $Z_j(\rho, \theta)$. The j is determined by:
- ordering the polynomial with lower radial order first
- and for given radial order the sine term is odd numbered and cosine term is even numbered. Converting between indices (especially from j to m and n) is useful because we generate the polynomials using two indices(m,n) and some formulae are written in terms of one index (j). A method of conversion between the two indices is given in Appendix D.

The generating function for Zernike polynomials is:

$$Z_n^m(\rho, \theta) = \begin{cases} \sqrt{\frac{2(n+1)}{1+\delta_{m0}}} R_n^{|m|}(\rho) sin(m\theta), if m \geq 0 \\ \sqrt{2(n+1)} R_n^{|}m|(\rho) cos(m\theta), if m < 0 \end{cases} \tag{1.16}$$

$$R_n^{|m|}(\rho) = \Sigma_{k=0}^{(m-n)/2} \frac{(-1)^k (n-1)!}{k![\frac{n+m}{2}-k]![\frac{n-m}{2}-k]!} \rho^{n-2k}, \quad with\, n \geq 2m\, and\, n - |m| an\, even\, number \tag{1.17}$$

Zernike polynomials are made up of terms that are of the same form as the types of aberrations often observed in optical tests. For example primary spherical aberration (SA)is the sum of terms of radial order 4, and secondary SA is (Z_6^0) and so on. The total SA is the sum of all orders of SA. Primary Coma is the two terms Z_3^1. Similarly other aberrations can be expressed as sum of appropriate polynomials.

Zernike polynomials are a complete set of polynomials in coordinates – ρ and θ and are orthogonal in a continuous function over the interior of a unit circle, and in general they will not be orthogonal over a discrete set of data points within a unit circle.

Zernike polynomials have three properties that distinguish them from other sets of orthogonal polynomials:
-They have simple rotational symmetry properties that lead to a polynomial product of the form $R[\rho]g[\theta]$ where $g[\theta]$ is a continuous function that repeats itself after every 2π radians.
-The radial function must be a polynomial in ρ of degree 2n and contain no power of ρ less than m.
-r$[\rho]$ must be even if m is even, and odd if m is odd (Wyant,2003).

1.5.1 Some advantages of modeling wave-front perturbations with Zernike polynomials

- Once we fit a wavefront with a certain number of terms and then fit the same wavefront with some more terms, the initially determined coefficients don't change after fitting more number of terms.
- The polynomial generating formula is the same irrespective of the size of aperture

- The mean value of each Zernike polynomial is zero (except piston term, whose mean value is 1). Thus the mean value of the wavefront to be fit is given only be the coefficient of the piston term.
- The variance over the polynomial is =1 for all polynomials. Thus the variance of the estimated wavefront is given by the sum of coefficients of the terms, which is very useful while calculating variances of phase screens.

Most of the advantages don't hold if the aperture is non-circular or is not a filled circle. Thus Zernike polynomials are useful only for fully filled apertures. The first 40 Zernike polynomials are shown in Figure 1.5. These were generated using MATLAB software.

1.5.2 Residual wave-front error after modeling J Zernike terms

When a phase screen is modeled in terms of a fixed number of Zernike terms, the residual phase variance σ^2 over a pupil of diameter d after fitting J terms is given by:

$$\sigma^2 = 0.2944 J^{-\sqrt{3}/2} (d/r_0)^{5/3} \tag{1.18}$$

Where

r_0 = Fried parameter. This holds good only for number of terms more than 15. The mean square wavefront error of an uncorrected wavefront is given by:

$$\sigma^2 = 1.031 * (D/r_0)^{5/3} \tag{1.19}$$

It can be found analytically using the formulae or Zernike polynomials that the tip-tilt correction alone can lead to 87% relative improvement in the mean square phase variance over the pupil. The plot of residual variance vs. number of terms is as shown in Fig.1.6
Since the wavefront is modeled as $\phi = \Sigma a_i Z_i$, making use of the orthonormal nature of the polynomials, one can write $a_i =$

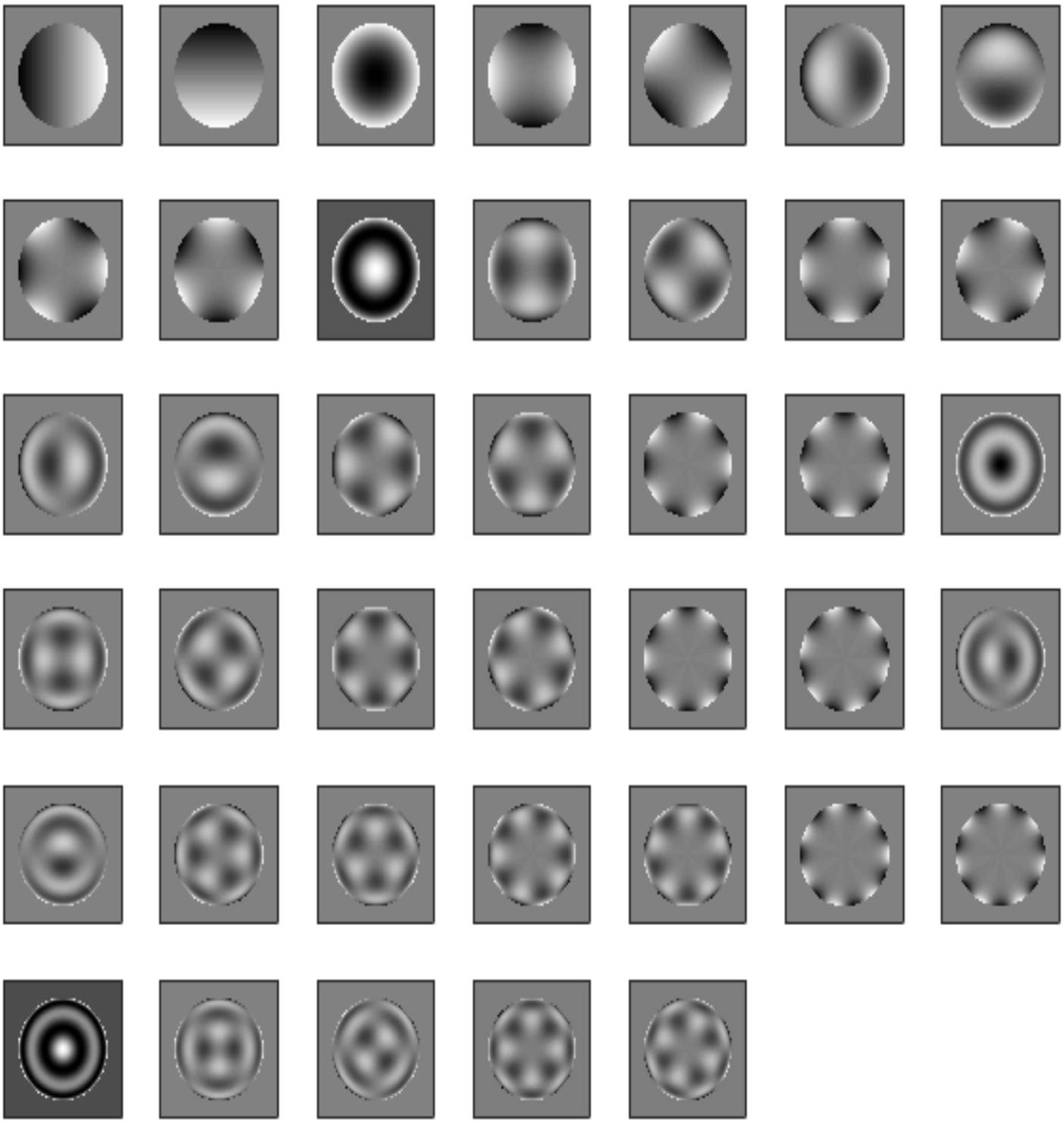

FIGURE 1.5: The first 40 zenike polynomials generated using MATLAB. Images are numbered left to right, top to bottom. Each image represents the zernike polynomial over a 50 cm aperture. Each pixel represents 1 mm, size of the image is, size of the in 128-by-128.

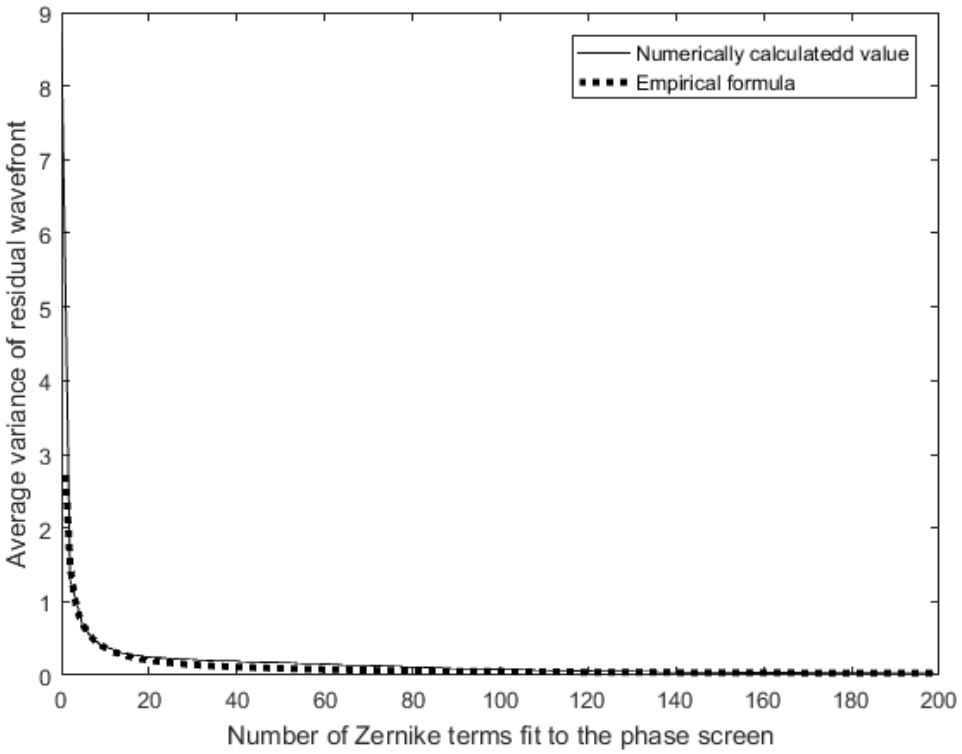

FIGURE 1.6: Residual variance of wavefront for phase screen of r_0=10 cm (numerically calculated and theoretical values are plotted).

$\int \phi Z_i ds$ where ds is an infinitesimal area in the region of the wavefront. This property can be made use of to calculate the covariance of the coeffficientss a_i.

Chapter 2

Solar Adaptive Optics

2.1 Methods Used

There are three possible methods of wavefront sensing in solar adaptive optics. They are: (1). Correlation Tracking Shack-Harttmann Wave-front Sensor (CT-SHWFS) (2) Quad-cell or quadrant detector (3) Limb tracking. In CT-SHWFS, the sub consecutive images to find the overall shift correction required, 2)In Quad-cell method the image is divided into 4 quadrants and intensity is measured in each quadrant, 3) In limb tracking method, the motion of a part of the solar image containing the solar limb is tracked.

In any stellar wave-front sensing system, the motion of the image centroid determined and the shift in centroid gives the tilt in the pupil. This method is not suitable for solar images because sun is an extended source and the centroid does not give the correct value of tilt required. We use CT-SHWFS for estimating the local and global slopes of the wave-front over the telescope pupil.

2.1.1 Correlation method (currently used)

Solar images are correlated to find the overall tip-tilt correction required. Correlation function is defined as:

$$h(\tau) = f(t) \times g(t) = \int_{-\infty}^{\infty} f(t)g(t+\tau)dt$$

whereas a convolution function is defined as:

$$h(\tau) = f(t) * g(t) = \int_{-\infty}^{\infty} f(t)g(\tau - t)dt$$

If we take the Fourier transform of the correlation function, we have:

$$h(\tau) = \int_{-\infty}^{\infty}[\int_{-\infty}^{\infty}\overline{F}(\gamma)e^{-2\pi\nu\tau}d\nu \int_{-infty}^{\infty}G(\nu')e^{-2\pi\nu'(t+\tau)d\nu'}]d\tau$$

$$= \int_{-\infty}^{\infty}\int_{-\infty}^{\infty}\int_{-infty}^{\infty}\overline{F}(\nu)G(\nu')e^{-2\pi(\nu'-\nu)\tau}e^{-2\pi\nu'(t)d\nu d\nu'}d\tau d\nu d\nu'$$

Thus $h(\tau) = \int \overline{F}(\nu)G(\nu')e^{-2\pi i\nu'\tau}[\int_{-\infty}^{\infty}e^{-2\pi i\tau\nu'-\nu)}d\tau]d\nu d\nu'$

$$= \int_{-\infty}^{\infty}\int_{-\infty}^{\infty}\overline{F}(\nu)G(\nu')e^{-2\pi i\nu'\tau}\delta(\nu'-\nu)d\nu' d\nu$$

$$= \int_{-\infty}^{\infty}\overline{F}(\nu)G(\nu)e^{-2\pi i\nu\tau}d\nu$$

$$= \mathcal{F}[\overline{F}(\nu)G(\nu)]$$

The correlation function h shows how similar the two functions f and g are. In our case f and g are consecutive solar images. The maximum of the correlation function shows the maximum similarity between the images and the location of the maximum shows the relative shift between the two images. Thus the coordinates of the maximum of the correlation function give the tilt correction to be applied to the image.

2.1.2 Quad cell

The image space is divided into 4 quadrants as in Fig 2.1. A reference intensity is fixed: it could be the intensity pattern of the first image. The shift in intensity relative to the reference gives the tip-tilt correction required. This method is not useful for solar images except for the case when there is an isolated small sunspot. However, an isolated small sunspot may not always be available, especially during the time of minimum activity in the sunspot cycle.

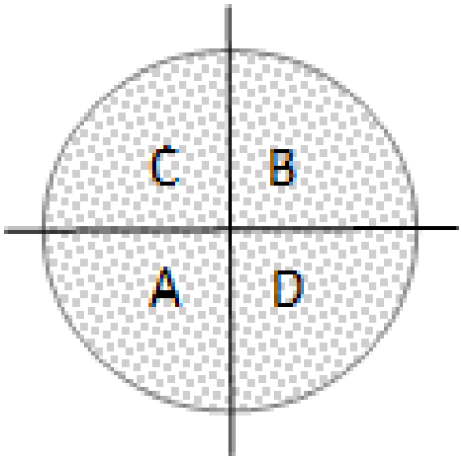

FIGURE 2.1: Image in Quad cell-image is divided into four quadrants

2.1.3 Limb tracking

A small part of the image containing the limb is tracked to determine the tip-tilt correction. This method also may be used for solar images.

Chapter 3

Solar Image Stabilization System

3.1 Experimental Setup of the Image Stabilization System

Figure 3.1 shows the laboratory setup of the proposed solar image stabilization system. A small ($\approx 15'' \times 15''$) portion of the solar image formed by the telescope is selected with a pinhole. The beam diverging from the pinhole is then collimated by a lens. An one-inch diameter flat mirror mounted on a piezo-electric actuator at angle of 45 degrees with respect to the collimated beam diverts the beam towards a beam splitter. The transmitted beam from the beam splitter is sent to be focused on to a CCD for observing the Sun (science camera), the reflected beam is focused onto a CCD to for calculating tip/tilt correction required. The setup is as shown below: Here the CCD for correction takes the

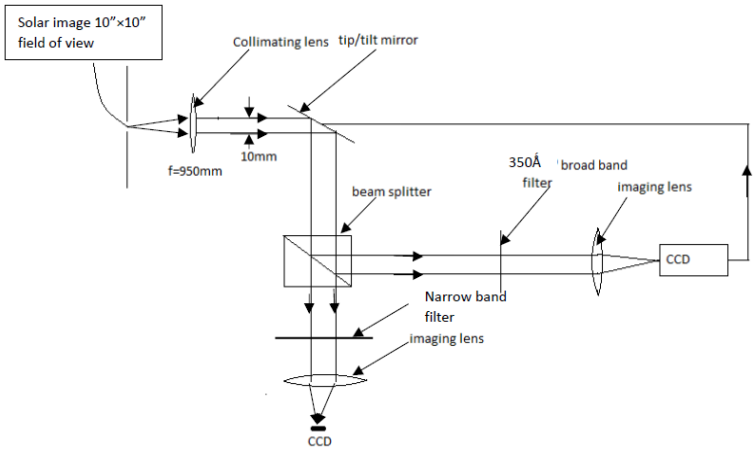

FIGURE 3.1: The experiment setup as used in the lab

images continuously during image acquisition and stores them in a computer. Consecutive images from the CCD are then correlated with a reference image and the relative shifts between

them are calculated. The shifts are then converted into incremental voltages using a predetermined calibration procedure. These voltages are then applied to the piezo-electric actuators following a control algorithm. The voltages thus applied to the actuators tilt the mirror at the pupil plane in such a way that the image motion at the image plane is arrested. Once the image motion is stabilized, the science camera can record long exposure images without significant loss due to image motion.

Before deploying such an image stabilizing system at the Kodaikanal Tower Telescope, we decided to do the system integration and testing at the adaptive optics laboratory at IIA, Bangalore. In the laboratory setup, the solar image will be replaced with a spatial light modulator containing solar images recorded at the site.

For the purpose of calibration, we illuminate the pinhole with a He-Ne Laser in the laboratory.

3.2 Identification of Components

As can be seen from the Figure 3.1, the components of the ISS are identified and listed as:

S.No	Component Name	Specification	Quantity
1	Lens	Diameter=50mm, Focal length $\sim$ 1m	3
2	Beam Splitter	50-50	1
3	Laser	He-Ne, 632.8 nm	1
4	Pinhole	0.5 mm	1
5	CCD	imaging, observing	2
6	Mirror	Diameter=25 mm	1
7	Piezoelectric Actuator	Range=150V in x and y axes	1

3.3 Design parameters of ISS for the KTT

The Kodaikanal Tower Telescope consists of a two mirror coelostat system, a 60 cm diameter flat mirror and a 38 cm diameter achromatic doublet. The coelostat consists of a two 60 cm optical flats housed on top of a 11 m tower. The primary mirror of the coelostat is rotated about an axis aligned with the north-south direction and is elevated at an angle equal to the latitude

of the place, at half the diurnal rate. The secondary mirror of the coelostat is adjusted such that the sunlight goes vertically down through the tower. A 60 cm flat mirror kept at angle of 45 degrees to the vertical at the bottom of the tower then directs the sunlight horizontally on to the achromatic doublet. The achromatic doublet forms a 38 cm image of the Sun at a distance of 36 m.

Before starting the experiment, we have estimated the approximate value of the parameters of the components (collimating and imaging lenses, piezo-electric stage) as follows:

The F-number of the telescope imaging system is 94.7.

The diffraction limited resolution of KTT at 500 nm is 0.33 arcsec ($1.22\lambda/D$, where λ is the wavelength and D is the diameter entrance pupil).

Plate scale or image scale of KTT = 1/focal length (in mm) = $206265 \times 1/36000$=5.7"/mm. We choose the width of the collimated beam as 10 mm. This choice leads the focal length of the collimating lens as f_c = 94.7 $\times$ 10 = 947 mm.

If choose the focal length of the imaging lens as 947 mm, the image scale at the image plane will be 5.7 arc-sec per mm. For a pixel size of 13 micron, a 3.3 mm image of the solar surface image will occupy about 256 pixels and will correspond to about 19 arc-sec field of view.

By slightly reducing the focal length of the imaging lens and the camera pixel size we can achieve a field-of-view of 15".

The measured mean square image motion the KTT is about 1.1 arcsec^2. Theoretically, this corresponds to r_0 of $\sim$ 4 cm at 550 nm. This approximately corresponds to about 5 μ rad. We have selected off-the shelf piezo-electric stage from *Piezosystemjena* (www.piezosystem.com). It has a maximum of $\pm$ 4 milli-radians tilt range and 0.02 μ radians resolution. This is well suited for our purposes.

3.4 Component Evaluation

3.4.1 The Actuator and its calibration

The Actuator
The actuator is a piezoelectric actuator. Thus it works according to the principle of piezoelectric effect. When a piezoelectric crystal is subjected to strain, it generates an electric potential difference across it. The potential difference may be in the same direction as the strain (longitudinal piezo-electric effect) or in a direction perpendicular to strain (transverse piezoelectric effect). The reverse effect also occurs: when a differential voltage is applied across the ends of a piezoelectric crystal, a differential strain is produced in the crystal. This way a single crystal produces a certain amount of strain and a stack of crystals, each with a voltage difference across their ends give a larger amount of strain. This strain is used to actuate the tip-tilt by attaching a mirror to one surface of the piezo-electric crystal.

Calibration The actuator has two input channels to input the voltage (one channel for tilt about each axis). After a mirror is mounted onto the actuator, we wish to know the following:
We need to know how much the mirror turns for a certain voltage applied in each channel. We also need to know about which axis the mirror is turning when a voltage is applied (rotation may not be along one axis only. Based on the position in which the actuator is mounted, the rotation may have components along two axes). The setup shown in 3.2 was used for the calibration of the actuators:

3.4.2 Procedure

- The components are assembled and aligned according to the setup.
- The CCD is connected to power supply and computer and neutral density filters are placed to prevent it from saturating.

FIGURE 3.2: Setup used in lab to calibrate response of actuator

- Through the ANDOR Solis software, the temperature of the CCD is set to -85^0C to bring down the levels of dark current.
- The actuator is connected to the PC
- Voltage is applied to one of the actuators in appropriately small steps and the respective images are taken.
- The changes in displacement of the image for changes in Voltage are as shown below 3.1:
- They are plotted as shown 3.3, 3.4
- The calculation is repeated for Voltage applied in other axis 3.2, 3.5, 3.6
- Next voltage was applied in steps in the other (perpendicular) direction and the shift of image in each direction is measured

V_x	Δx	Δy
-15	–	–
-10	-32.33	1.4
-5	-66.36	1.86
0	-100.92	2.31
5	-135.33	2.5
10	-170	3.09
25	-204.7	3.7
20	-239.33	4.22
25	-273.62	4.62
30	-307.86	4.86
35	-341.5	5.33
40	-375.2	5.8
45	-408.25	6
50	-440	6.3
55	-471.5	6.5
60	-500	7

TABLE 3.1: Shift in position of image for voltage applied along the first axis

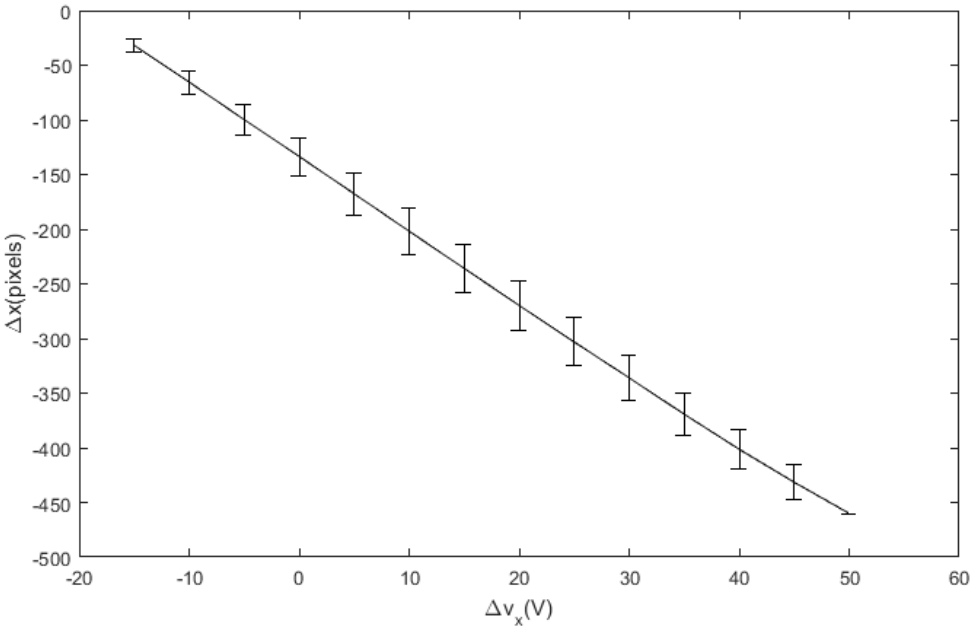

FIGURE 3.3: Plot of shift of image in x direction vs. voltage applied along first axis. The small vertical lines are error bars

The interaction matrix of the actuators is given by 3.1

$$\begin{bmatrix} \Delta x \\ \Delta y \end{bmatrix} = \begin{Bmatrix} a_{11} & a_{12} \\ a_{21} & a_{22} \end{Bmatrix} \begin{bmatrix} \Delta V_x \\ \Delta V_y \end{bmatrix} \tag{3.1}$$

V_y	$\Delta\mathbf{x}$	$\Delta\mathbf{y}$
15	–	–
20	0.75	46.17
25	0.45	91.36
30	0.2	136.8
35	-0.11	182.22
40	-0.38	227.62
45	-0.43	273.14
50	-1	318.67
55	-1.2	363.8
60	-1.5	408.75
65	-1.67	453.33
70	-2	498.5

TABLE 3.2: Table of specifications-Lens1, average f=988.7mm, std. deviation=2.1

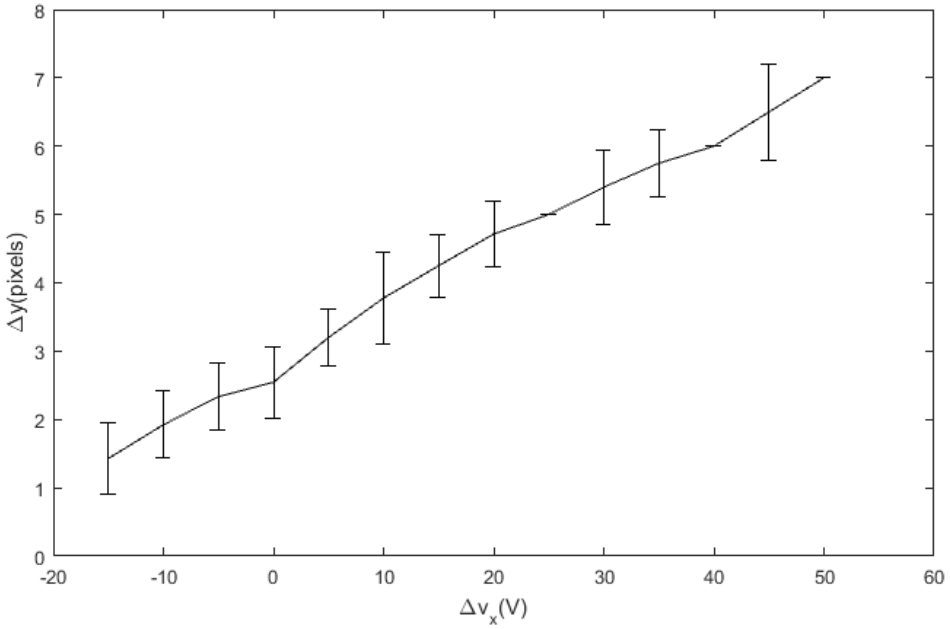

FIGURE 3.4: Plot of shift of image in y-direction vs. change in Voltage in x-direction

Thus a_{11}=-6.7579
a_{12}=-0.0017
a_{21}=-0.1288
a_{22}=9.1048
The control voltages to be applied to the actuator are estimated as the product of control matrix and estimated shifts. The control matrix is obtained by inverting the interaction matrix as

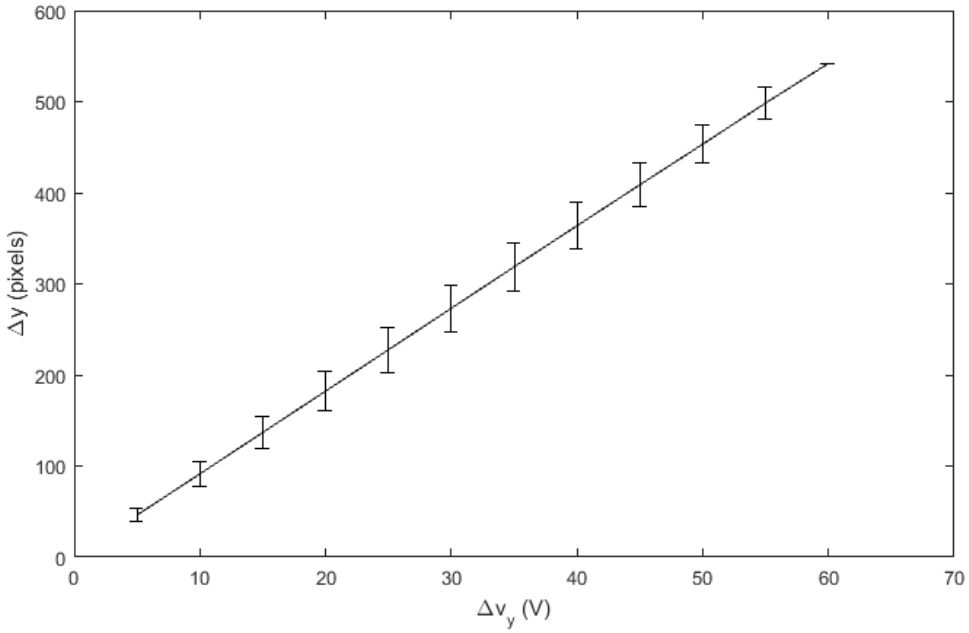

FIGURE 3.5: Plot of shift of image in y-direction vs. change in Voltage in x-direction

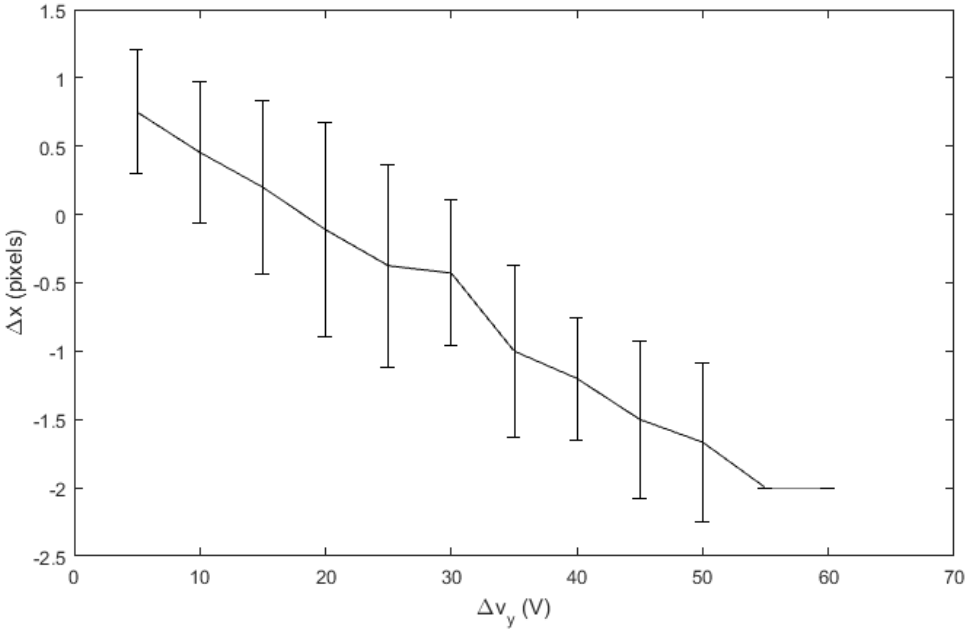

FIGURE 3.6: Plot of shift of image in y-direction vs. change in Voltage in x-direction

shown in Eq. 3.2

$$\begin{bmatrix} \Delta V_x \\ \Delta V_y \end{bmatrix} = \begin{Bmatrix} -0.148 & -0.00003 \\ -0.002 & 0.109 \end{Bmatrix} \begin{bmatrix} \Delta x \\ \Delta y \end{bmatrix} \tag{3.2}$$

3.4.3 Measurement of focal lengths of the Lenses

As shown in setup, two lenses of focal length$\sim$ 1000 mm and diameter 50 mm were used. A set of readings of object distance (u) and image distance (v) were noted for each lens to verify their focal lengths as shown in tables 3.3, 3.4

S.No	u (mm)	v (mm)	f (mm)
1	2000	1960	989.9
2	1900	2070	990.7
3	1800	2200	990
4	1850	2120	987.9
5	1950	1990	984.9
6	2000	1960	989.9
7	1950	1990	984.9
8	1900	2070	990.7
9	1850	2120	987.9
10	1800	2200	990

TABLE 3.3: Table of focal length measurement-Lens1, average f=988.7mm, std. deviation=2.1

S.No	u (mm)	v (mm)	f (mm)
1	2000	2050	1012.3
2	1950	2080	1006.4
3	2050	1980	1007.2
4	1900	2160	1010.8
5	1850	2210	1007
6	2000	2050	1012.3
7	1950	2090	1008.8
8	2050	1980	1007.2
9	1900	2160	1010.8
10	1850	2210	1007

TABLE 3.4: Table of focal length measurement-Lens2, average f=1009mm, std. deviation=2.24

3.5 Uncertainty of measurement

Focal length of a lens is given by $\frac{1}{f} = \frac{1}{v} - \frac{1}{u}$ where u is negative according to the sign convention used. Thus $\frac{1}{f} = \frac{1}{v} + \frac{1}{u}$ if all values are measured as positive. Here v and u are measured.

The uncertainty in the measurement of f is given by:

$$\Delta f^2 = [\frac{v^4}{(u+v)^4}]\Delta u^2 + \frac{u^4}{(u+v)^4}\Delta v^2 \tag{3.3}$$

In this case, $\Delta u = \Delta v = 1mm$. The values are substituted in the above formula and the average uncertainty in the measurements turns out to be = 0.35mm

3.6 Depth of focus

The image detected anywhere within this region is

$$d = 2 \times (\frac{f}{a})^2 \times \lambda \tag{3.4}$$

which is equal to 9mm.

Chapter 4

Summary & Future work

As all the opto-mechanical components could not be procured on time, I could not complete the project. Nevertheless, I have throughly studied the basics of a correlation tracking wave-front sensor and an image stabilization system both theoretically and through computer simulations. In what follows, I enumerate the list of things that have been completed and those that are pending.

List of completed tasks:

1. Design of the system parameters.
2. Procurement of the major components.
3. Calibration of for the tip/tilt actuator.
4. Procedure to estimate the global wave-front tilt using CT-SHWFS.

List of tasks to be accomplished:

1. Developing an integrated software for image acquisition, estimation of relative shifts and the corresponding control voltages.
2. Developing a control software suitable for closed loop operations with suitably tuned digital PID controller.
3. Demonstration of the closed loop operation in the lab with solar images loaded in SLMS. SLMs are yet to be procured.
4. Deploying the system at KTT and evaluating the performance.

Prospects for a Ph. D. Thesis:

1. Once the image stabilization system is deployed, the project can be continued to develop and deploy a low order adaptive optics system.

2. Next, an high order AO system can be developed to enhance the Strehl ratio (contrast in the case of solar images) further.

3. This can further be followed up by the development of multi-conjugate AO system that corrects over a wide field of view.

Appendix A

Simulation of Point Spread Function for a given r_0

A.1 Introduction

The atmosphere through which the light from a celestial object propagates is turbulent and distorts the wave front. Thus the image quality is significantly deteriorated.

A.2 Creating a phase screen

Phase screen: A phase screen is the atmospheric path length fluctuations over a region of space. Wave front is a surface of constant phase. Mathematically wave front is represented by a complex number (e.g., $Ae^{i\phi}$). Phase screens occur in real and complex pairs. We are interested only in the real part of the phase screen since that is the one which is measured.
The spatial power spectrum $\Phi(k)$ which was given by Kolmogorov is:

$$\Phi(k) = 0.023 r_0^{-5/3} k^{-11/3} \tag{A.1}$$

Here k is spatial frequency, r_0 is Fried parameter.

Then we created 3 phase screens of side 40.98m were created. The phase screens are shown below.

A.3 Point Spread Function:

The point spread function is obtained through the following steps:

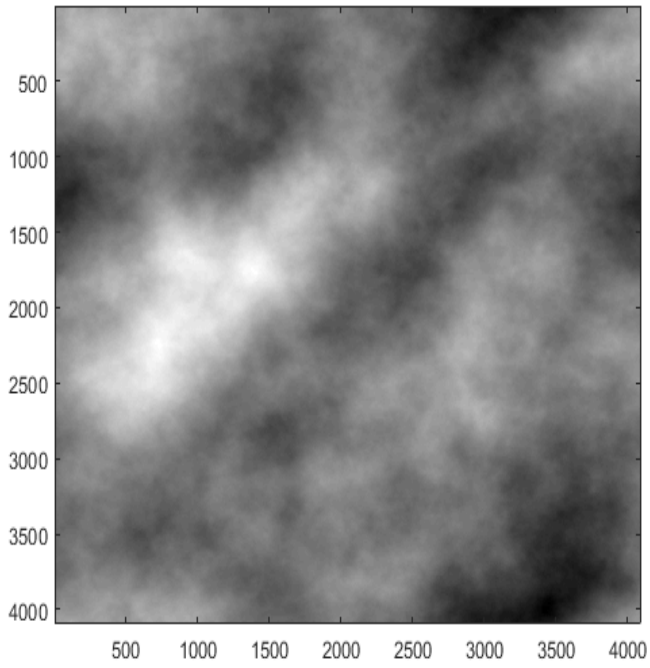

FIGURE A.1: Phase screen of size 40.96 m for r_0=0.1 m with each pixel=1 cm

- An aperture function w is created: w=1 if radial coordinate <= R, 0 if radial coordinate >R, where R is the radius.
  In this case the radius is taken to be R = 19 cm to match with that of KTT.
- The aperture function superposed on a phase screen gives the phase fluctuation over the aperture.
- Instantaneous intensity PSF is given by

$$PSF = |\mathcal{F}(f)|^2 \tag{A.2}$$

  where f is the phase function
- The aperture function is shifted along the phase screen and the superposed apertures represent the phase over the aperture at different times. The average PSF of many instantaneous PSFs is calculated and shown.

The shapes of actual PSF A.7 and ideal psf A.8 are shown.

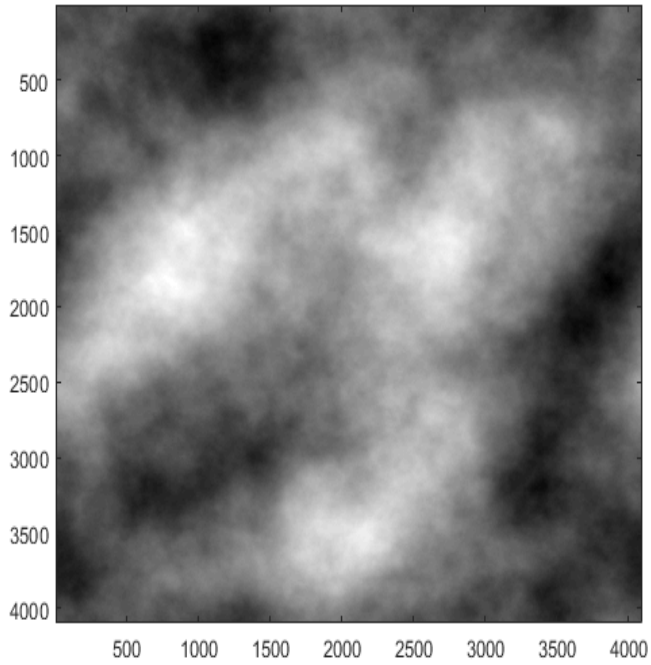

FIGURE A.2: Phase screen of size 40.96 m for r_0=0.15 m with each pixel=1 cm

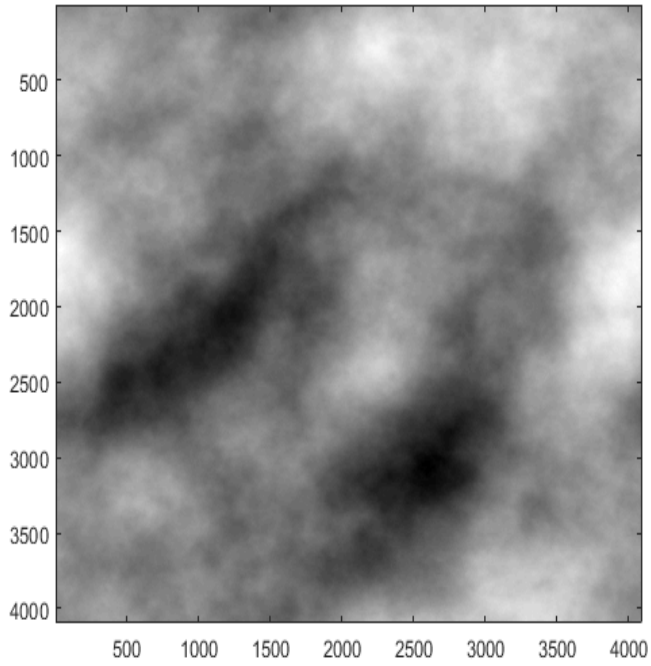

FIGURE A.3: Phase screen of size 40.96m for r_0=0.2 m with each pixel = 1 cm

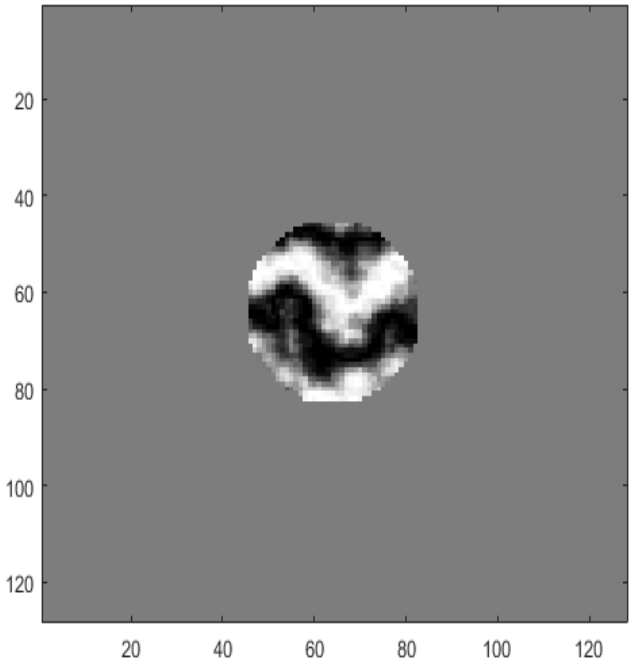

FIGURE A.4: Real part of complex wavefront over a 38cm diameter aperture with each pixel=1cm

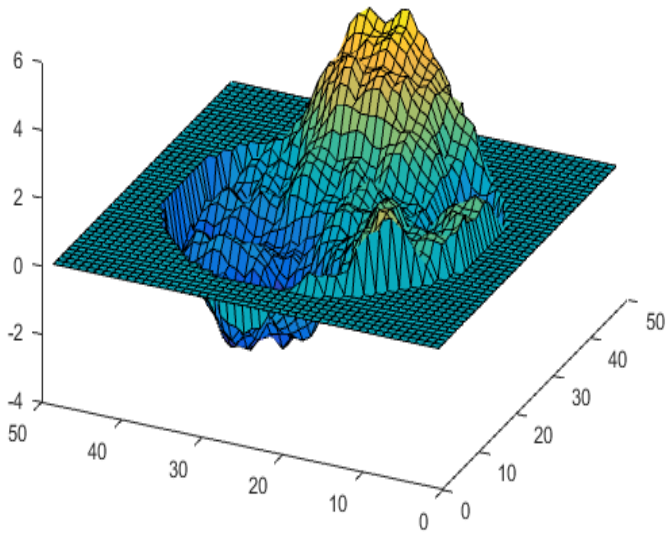

FIGURE A.5: Real part of complex wavefront over a 38cm diameter aperture with each pixel=1cm. r_0 = 20 cm.

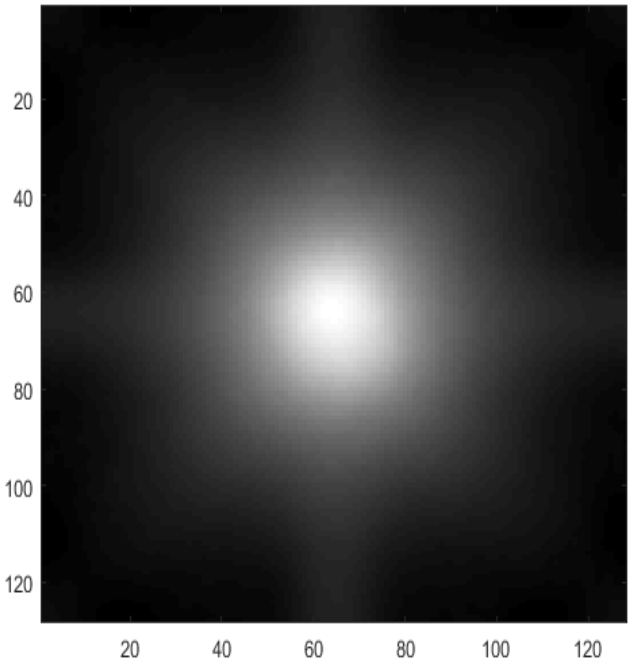

FIGURE A.6: Average Point spread function for r_0=0.1m; 1 pixel =

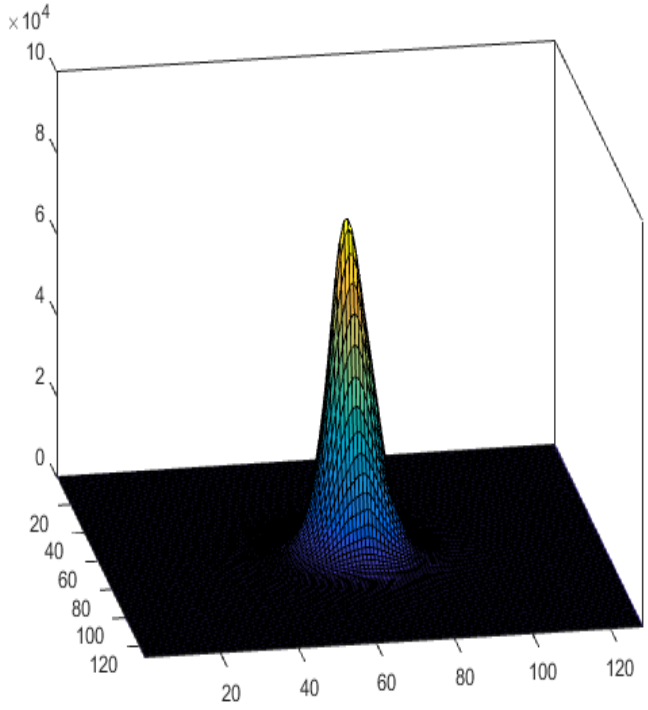

FIGURE A.7: 3D shape of a PSF of an aperture of diameter 38 cm and r_0 =20 cm

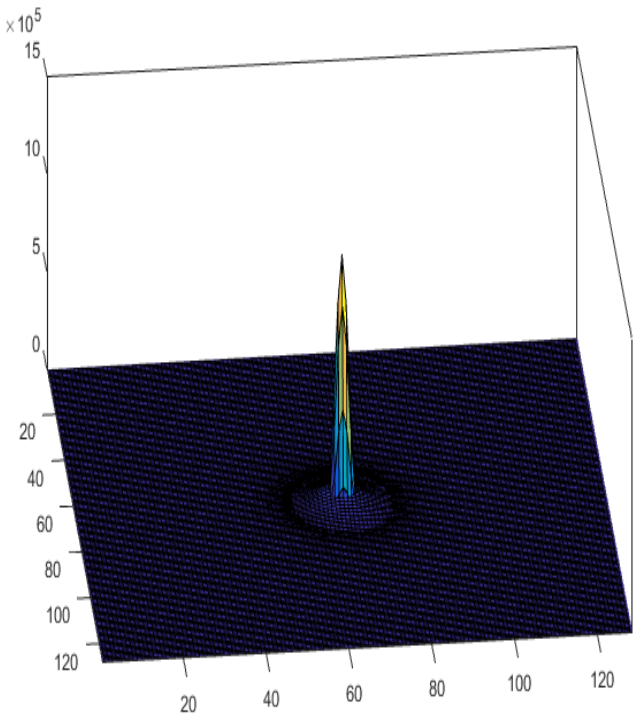

FIGURE A.8: 3D shape of an PSF of an aperture of diameter 38 cm (formed by a flat wavefront, does't depend on r_0).

Appendix B

Assessment of phase screens

B.1 The R.M.S fluctuations of phase

As shown in previous chapter, a phase screen is a plot of fluctuations of phase over a region. The Fried parameter can be used to indicate how good the seeing condition happens to be. Generally, the magnitude of phase fluctuations increases with decreasing Fried parameter r_0. In the phase screens simulated in the previous chapter the values in a row across the plot are plotted and their r.m.s value is calculated for each phase screen as show in figure.

B.2 The phase structure function

The phase structure function is defined as the mean square variance of phase. According to the empirical law of Kolmogorov power spectrum, the phase structure function is expressed as

$$D_\phi(r) = 6.88(\frac{r}{r_0})^{5/3} \tag{B.1}$$

The phase structure function can also be measured across a region using

$$D_\phi(r) =< |\phi(x) - \phi(x+r)|^2 > \tag{B.2}$$

x is the location in space, r is the distance for which D_ϕ is calculated, ideally all possible x's have to be averaged.

B.3 Full Width at Half Maximum of PSF

FWHM: The width of the plot measured between those points with value = 1/2 of function's maximum value. It is a measure

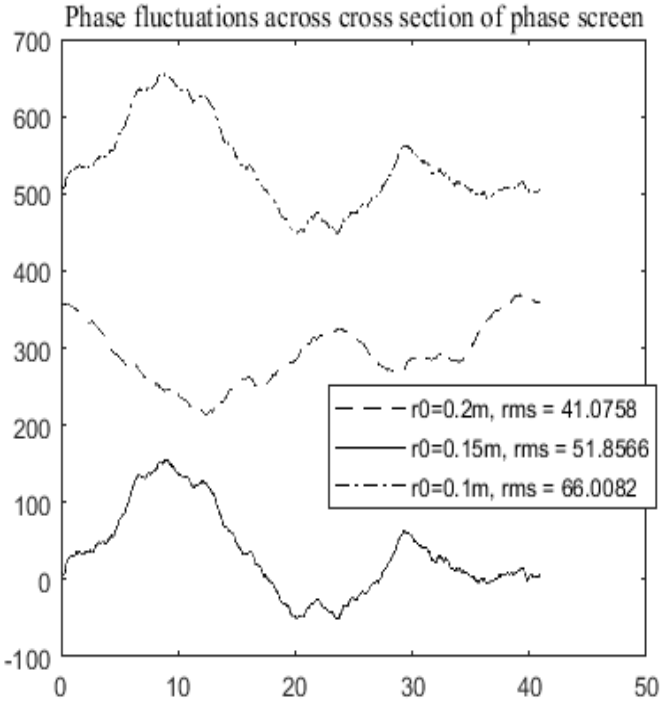

FIGURE B.1: Phase fluctuations (in rad) over the length of the phase screen and their rms values for 3 values of r_0. The plot for each r_0 is offset by a certain constant value for clarity. Thus only the magnitude of fluctuations (not the total value along the y-axis is significant.

of the extent of the function. A plot of cross section of the PSF is shown. The FWHM of the PSF according to theory is

$$0.98(\frac{\lambda}{r_0}) \tag{B.3}$$

Here λ is 550 nm and r_0 is 0.1 m. Thus FWHM = 0.56". No. of pixels per diffraction limit = $\frac{128}{38}$ = 3.36.
Diffraction limit of telescope = $1.22\frac{\lambda}{D}$ = 0.331".
1 pixel = $\frac{0.331}{3.36}$ = 0.108". Therefore theoretically FWHM in pixels = $\frac{1.12}{0.108} = 10.36$ pixels
In the plot, FWHM = 12 pixels.

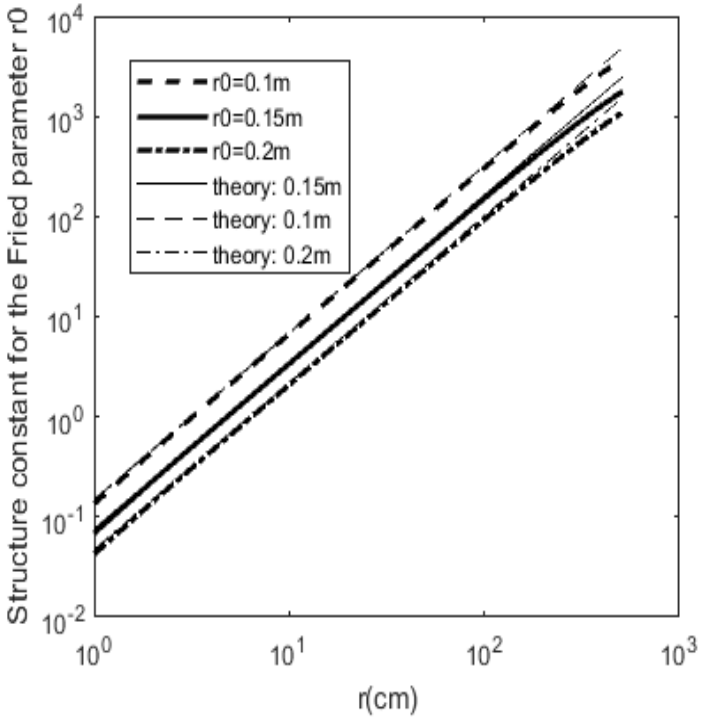

FIGURE B.2: Simulated and theoretical plots of the phase structure function over a distance of 5 m

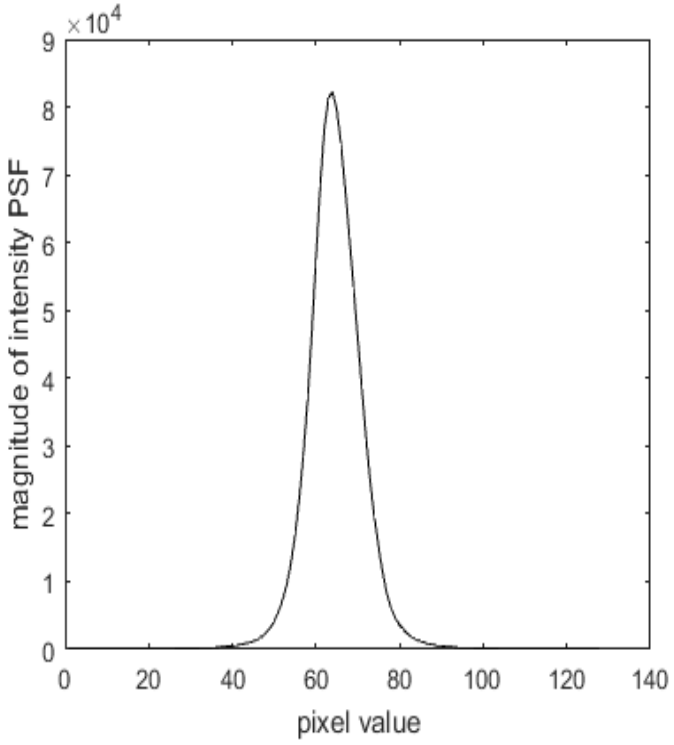

FIGURE B.3: Plot of magnitude of PSF across its cross section, r_0=0.1 m

Appendix C

Creation of phase screen by identifying the Zernike polynomial series

Aim: To create a phase screen using Zernike polynomials: $\Sigma a_i Z_i$.

In order to do so, the Zernike coefficients a_i must be determined. They can be derived by first calculating the residual error after correction for a certain number of modes. The coefficients were first obtained by Fried(1988) for polynomials defined by Fried. Using the properties of Zernike polynomials, it can be written, as shown in Noll(1975), the covariance matrix of zernike coefficients a_j in the Fourier domain(with radial coordinate k) can be written as:

$$< a_j a_{j'}^* >= (0.046/\pi)(R/r_0)^{5/3}[(n+1)(n'+1)]^{1/2}(-1)^{(n+n'-2n)/2}\delta mm' \times \int k^{-8/3}\frac{J_{n+1}(2\pi k)J_{n'+1}(2\pi k)}{k^2}dk \qquad \text{(C.1)}$$

r_0: Fried parameter,
$J_n(k)$ is bessel funtion of n^{th} order at location k.
Here j is the index of the Zernike polynomials numbered consecutively from 1, n and m are another type of indices of Zernike polynomials depending on degree of radial polynomials. It is shown in Appendix C how to convert one notation to the other.

This integral has to be solved to obtain the covariance matrix.

In the same paper Noll(1975) it is shown that

$$I_{nn'} = \int_0^\infty k^{-8/3} \frac{J_{n+1}(k) J_{n'+1}(k)}{k^2}$$

$$= \frac{\Gamma(\frac{14}{3}\Gamma[(n+n'-\frac{14}{3}+3)/2]}{2^{14/3}\Gamma[(-n+n'+\frac{14}{3}+1)/2]\Gamma[(n-n'+\frac{14}{3}+1)/2]\Gamma[(n+n'+\frac{14}{3}+3)/2]} \quad \text{(C.2)}$$

where Γ is the Gamma function.
From this the integral in the covariance formula can be calculated to be $= < a_j a_{j'} >= (0.046/\pi)(R/r_0)^{5/3}[n=1)(n'+1)]^{1/2}(-1)^{(n+n'-2n)/2}\delta$
Thus we can obtain the covariance matrix of Zernike coefficients upto any specified j. Next we obtain a set of Gaussian distributed random variables with a covariance matrix specified by $< a_j a'_j >$ for the element jj′ and mean zero.

Finally the wavefront is constructed from $\phi = \sigma_{i=1}^{n} a_i Z_i$. The program for generation of Zernike coefficients was written in Matlab as shown below:

C.1 Matlab Code

```
clear b coa coa1
clc
r0 = 5;
c=(0.046/pi)*(19/10) ∧ (5/3)*(2*pi)∧(11/3);
k=0:0.1:21;

for n=1:9
  b(n,:)=besselj(n,2*pi*k);
end       %gives n*k matrix with n as order of bessel function of first
kind, k is variable argument if besel function
for j=1:40
  r=roots([1/2,3/2,-j]);
  n=double(ceil(vpa(max(r),5))); %to find n of the zernike polyno-
mial corresponding to row
  if rem(n,4)==1 | |rem(n,4)==2 %this if loop is to find the m's
```

```
    if xor(rem(j,2),rem(n,2))
    m=double(j-n*(n-1)/2-n);
  else
    m=double(j-n*(n-1)/2-n+1);
  end
  else
    if xor(rem(j,2),rem(n,2))
      m=double(j-n*(n-1)/2-n+1);
    else
      m=double(j-n*(n-1)/2-n);
    end
  end
  for j1=1:40 % to create 27*27matrix if we require 27 Zernike polynomials, I have arbitrarily chosen 27 Zernike polynomials
    r1=roots([1/2,3/2,-j1]);
    n1=double(ceil(vpa(max(r),5))); %to find n of zernike polynomial corresponding to column
    if rem(n,4)==1 ||rem(n,4)==2
      if xor(rem(j1,2),rem(n1,2))
        m1=double(j1-n1*(n1-1)/2-n1);
      else
        m1=double(j1-n1*(n1-1)/2-n1+1);
      end
    else
      if xor(rem(j1,2),rem(n1,2))
        m1=double(j1-n1*(n1-1)/2-n1+1);
      else
        m1=double(j1-n1*(n1-1)/2-n1);
      end
    end
    if m==m1 %since the kronecker delta occurs in the equation
      jj=b(n+1,:).*b(n1+1,:);
      ij=integrate(jj);
      ij=ij(end);
      coa(j,j1)=c*((-1)^ ((n+n1-2*n)/2))*ij*sqrt((n+1)*(n1+1)); %eq 2.5 as in Noll's paper
```

```
      coa1(j,j1)=double(c*((-1)^ ((n+n1-2*n)/2))*sqrt((n+1)*(n1+1))*gamma(14/
14/3+3)/2)/(2^ (14/3)*gamma((-n+n1+14/3+1)/2)*gamma((n-
n1+14/3+1)/2)*gamma((n+n1+14/3+3)/2)));
     else
      coa1(j,j1)=0; %eq2.5
      coa(j,j1)=0;
    end
  end
  [j,n,m]% to count/display j,n,m, can be commented
end

figure,contour3(coa1) an=mvnrnd(zeros(size(coa,1),1),double(coa1).*eye(size(
%to get the gaussian distributed variables which will be coefficients ai
```

C.2 Result

A plot of $a_i's$ looks likeC.2:

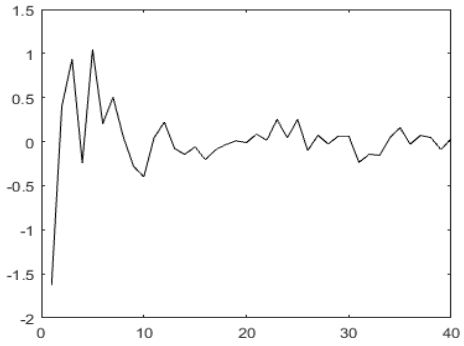

FIGURE C.1: Plot to show magnitudes of Zernike coefficients

According to Fried(1988), the tip and tilt (linear corrections) contribute to 87% of all the corrections. It can be seen in the figure above that the first two terms are much larger in magnitude than the rest and the magnitude decreases with higher order of the terms.
Next a phase screen is constructed using the Zernike coefficients obtained:

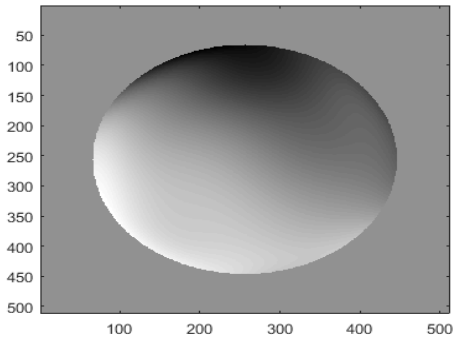

FIGURE C.2: Wavefront created from the $a_i's$

C.3 Verification

In this section it is verified whether the coefficients generated as random numbers produce a phase screen of r_0 close to the r_0 used to generate the coefficients.
According to the definition of r_0, the mean square variation of phase over a region of diameter 5cm = r_0 is 1.
The figure of wavefront shown above represents the phase over an aperture of diameter 38cm. 1mm is scaled to 1pixel. Here the mean square variation of phase over a region at of diameter 50 mm (=r_0), (which is 50 pixels) situated at the center is calculated.

In the simulated wavefront, variation over a circle of diameter 60 mm$\sim$ 1. The reason may be the limited number of Zernike terms calculated.

Appendix D

How to convert the index of Zernike from single index notation j to two indices n & m

When creating Zernike polynomials the notation R_n^m was used(as shown in previous apppendix). The polynomials can also be numbered sequentially starting from 0 (piston).

Thus the polynomials fit into a table as shown below:

TABLE D.1: Zernike polynomial indices: column and row headings are n and m respectively, the entries are j

m | n	**0**	**1**	**2**	**3**...
0	0		3	
1		1,2		6,7
2			4,5	
3				8,9

For odd n, the m's start from 1 and take the values of all odd numbers upto n. For even n, the m's start from 0 and take the values of all even numbers upto n.

For any m=0, there is 1 term for one value of n. For any n and for any m not equal to 0, there are 2 terms corresponding to cosmθ and sinmθ.

D.1 Determination of n

Consider any odd value of n. The number of terms with index n are $2(\frac{n+1}{2}) = N + 1$.

Consider any even value of n. The number of terms with index N are $2(\frac{N}{2}) + 1 = N + 1$.

Happily the same formula for number of terms corresponding to a particular value of n is the same irrespective of whether n is even or odd. Then applying the summation over n+1 to get the number of terms with n less than or equal to N, we get $J = \sum_1^N (n+1) = \frac{N(N+1)}{2} + N$. This is the case if we count all the m's of n=N. But we may stop at m=M. So we count the all the m's upto N-1:$j_1 = \sum_1^{N-1} (N+1) = \frac{N(N-1)}{2} + N - 1$.

Thus

$$\frac{N^2}{2} + \frac{N}{2} = J$$

has to be solved for n. Say each n corresponds to maximum M values of m. Then a particular j may or may not correspond to the last value of m. So the floor value of n obtained from the quadratic equation has to be taken. Or one can solve the equation

$$\frac{N^2}{2} + \frac{3N}{2} = J$$

and the ceil of n has to be taken.

D.2 Determination of m

If n is odd, there are $\frac{N+1}{2}$ values of m and if n is even, there are $\frac{N}{2} + 1$ values of m. In both cases, the number of terms with index N and m upto M = M+1 if both the $sinM\theta$ and $cosM\theta$ terms are counted. and = M if either $sinM\theta$ or $cosM\theta$ is counted. But given only a value of j, we cannot determine which is the case. So it has to be determined from other trends in the table. So far there are 2 formulae: $m = j - \frac{n(n-1)}{2} - n + 1$ and $m = j - \frac{n(n-1)}{2} - n$.

From the table we write down which formula is applicable depending on whether j is odd and whether n is odd as follows:

It can be seen that:
For n=1,2,5,6...
If both n and j are odd and if both n and j are even, the first formula applies.
If either n or j but not both are odd, the second formula applies.

For n==3,4,7,8...
If both n and j are odd and if both n and j are even, the second formula applies.
If either n or j but not both are odd, the first formula applies.

Appendix E

Results of measurements of some lenses

S.No	u (mm)	v (mm) f (mm)	
1	1800	2570	1058
2	1800	2585	1061
3	1850	2450	1054
4	1850	2450	1054
5	1900	2410	1062
6	1900	2430	1066
7	1950	2325	2295
8	1950	2295	1054
9	2000	2270	1063
10	2000	2280	1065
11	2050	2250	1073
12	2050	2230	1068
13	2100	2170	1067
14	2100	2175	1068
15	2150	2050	1049
16	2150	2045	1048
17	2200	2070	1066
18	2200	2060	1064
19	2250	1990	1056
20	2250	1985	1055

TABLE E.1: Table of specifications-Lens1, average f=1061mm, std. deviation=6.66

It is noted that Lens2 has an amount of astigmatism. The horizontal and vertical lines of the object are focused at different distances:

The astigmatism is reduced by reducing the aperture diameter of the lens,. Thus:

S.No	u (mm)	v (mm)	f (mm)
1	1700	1935	905
2	1700	1940	906
3	1750	1860	902
4	1750	1840	897
5	1800	1810	902
6	1800	1810	902
7	1850	1750	899
8	1850	1745	898
9	1900	1710	900
10	1900	1720	903
11	1950	1635	889
12	1950	1640	891
13	2000	1550	873
14	2000	1560	876
15	2050	1684	925
16	2050	1685	925
17	2100	1630	918
18	2100	1640	921
19	2150	1815	948
20	2150	1815	984

TABLE E.2: Table of specifications-Lens2, average f=910mm, std. deviation=28

S.No	u (mm)	v (mm)	f (mm)
1	1700	2080	935
2	1700	2090	937
3	1750	2015	936
4	1750	2010	936
5	1800	1935	932
6	1800	1940	934
7	1850	1880	932
8	1850	1860	927
9	1900	1825	931
10	1900	1830	932
11	1950	1760	925
12	1950	1780	930
13	2000	1750	933
14	2000	1750	933
15	2050	1710	932
16	2050	1700	929
17	2100	1660	927
18	2100	1680	933
19	2150	1635	929
20	2150	1635	929

TABLE E.3: Table of specifications-Lens3, average f=932mm, std. deviation=3.22

Appendix F

Actuator Specifications

F.1 Working the actuator

The actuator has two rotational degrees of freedom. The actuator has two input voltages for each direction of rotation, each of which is applied through controller(evd300). Physically, the amplifier for the actuator F.1 and actuator F.2 look as shown

FIGURE F.1: Amplifier evd300-it amplifies the signal sent from the computer before applying it to the actuator

F.2 Starting up the power supply

- Open packaging of the evd300 and set it on its stand with display facing front. Connect the power cable from the socket at the back to the mains supply and switch on the power switch of the evd30.
- Press the on/off switch beside the front display-all the LED's will glow for a few seconds indicating the self test and software set automatically performed by the EDS. Then a single green LED glows steadily without flickering indicating that evd300 is ready for use.

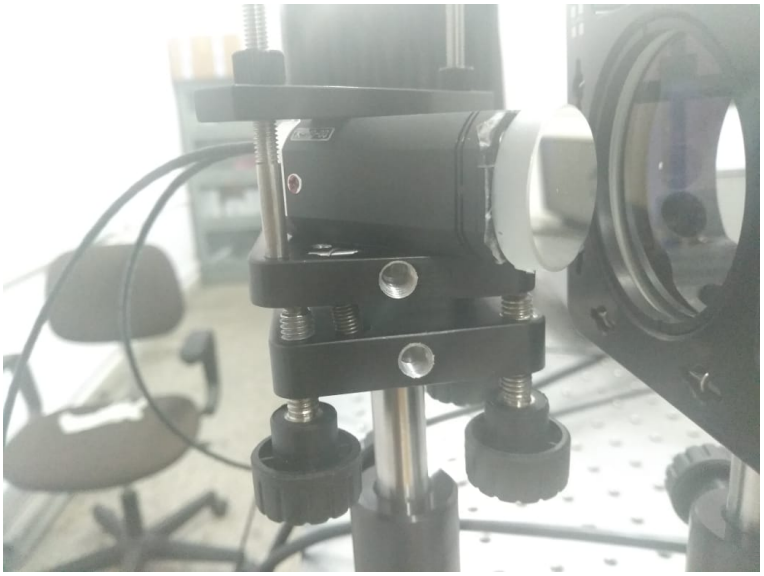

FIGURE F.2: The actuator with mirror attached and mounted

- The knob below the display is a potentiometer control for the input voltage.
- Initially upon switching on, the display shows -20V. This is the default input voltage of the EDS.
- Turn the potentiometer knob clockwise to increase the voltage upto 130V and then in anticlockwise direction upto -20V.
- Thus the evd300 and its power supply is working
- Switch off the EDS by pressing the on/off switch beside the display for more than two seconds
- Switch off power supply to evd300 by switching off the black switch at the back.
- Caution: If the actuator is idle for more than 24 hrs, it is advisable to switch off power supply from the mains.

F.3 Attaching the mirror

A double-sided tape may be used to attach mirror above the actuator. Stick tape neatly on black surface around the center of the top surface of the actuator and place mirror over tape.

Caution: Do not at any time apply considerable pressure directly on the actuator or on the sides of the actuator.

F.4 Applying voltages to the mirror

The actuator needs to be connected to the EDS via the coaxial cables provided for the purpose. Each cable is for voltage along each axis. Each cable has to be connected to each EDS. While connecting cables, the red dot on the cable from actuator must be aligned with red dot on cable form EDS. Once the cables are connected, the voltages displayed on the EDS are applied to the actuator.

F.5 Operating via computer's hyperterminal

Notice that the evd300 has two kinds of ports and may be connected to a computer through either of them:
RS232 port
ftd2 port
We have connected the actuator via the USB port using the appropriate cables provided. In the computer, it can be seen that two com ports are connected(for each axis).
Using hyperterminal: To operate it from a windows computer, a hyperterminal may be downloaded and installed. After installing the hyperterminal, select the port to which EDS is connected. The following are some of the commands (which are be used more frequently) which may be typed in hyperterminal:
The commands are supposed to be typed as: command,channel,value and the command gives the value to the channel. If the value is not specified, the command shows the existing value.

Command	**meaning/output**
stat	sets the value of Voltage(open loop) or microns displacement(closed loop)
mess	measures the value in the channel
ktemp	sets the temperature in degree Celsius
fan	switches the fan on(1) off(0)

TABLE F.1: table showing some of the commands which may be used in hyperterminal

Using Matlab:

In order to operate from Matlab, first some assembly files need to be loaded in workspace. Assembly files usually have the extension .dll. The following are some of the commands used:

1. The commands to load the appropriate assembly files are:
   asm1 = NET.addAssembly('c:\PSJ\piezojenad-Drive\Piezojena.Protocols.dll')
   asm2 = NET.addAssembly('c:\PSJ\piezojenad-Drive\Piezojena.Ftd2xx.dll')
   asm3 = NET.addAssembly('c:\PSJ\piezojenad-Drive\Piezojena.Visa.dll')
   asm4 = NET.addAssembly('c:\PSJ\piezojenad-Drive\Piezojena.Protocols.Ddrive.dll')
   The commands create 4 assembly variables called asm1, asm2, asm3 and asm4 of type dll.

2. Next certain call commands have to be activated. For this the call constructor command has to be given:
   service = Piezojena.Protocols.Ddrive.DdriveServices();

3. Next the device has to be connected. in this step the port where the actuator is connected needs to be specified: ddrive = service.ConnectDdriveToSerialPort('COM1');
   This is a function with argument COM1. It creates a variable called 'ddrive' which is of variable-type 'drive'. This command connects 'ddrive' to COM1.

4. To set a desired voltage in the channel,
   ddrive.SetDesiredOutput(0, 10)
   This function has two arguments (0 and 10). The first argument specifies the slot to which voltage is applied(we are only concerned with slot 0). The next argument specifies the amount of voltage to be applied (10). But if the oop is closed, the second argument specifies the required displacement.

5. Once we have completed operating the port, we have to disconnect the drive variable from the port:
   ddrive.Dispose()

The above commands can be used as part of an integrated code for implementing tip-tilt correction. They have been used in a loop to increment the input voltage in steps for calibration experiment.

Appendix G

References

1. http://www.ctio.noao.edu/ atokovin/tutorial/intro.html
2. F.Roddier, “Effects of atmospheric turbulence in optical astronomy”, Progress in optics, Vol.9, 1981
3. M.Born and E.Wolf, “Principles of Optics”, 6th Ed, Pergamon press, 1986
4. J.C.Wyant, “Zernike Polynomials for the Web”, 2003
5. W.Schmidt et al., “The GREGOR solar telescope on Tenerife”, arXiv:1202.4289v1 [astro-ph.IM], 20 Feb 2012
6. C.Denker et al., “Adaptive Optics at the Big Bear Solar Observatory: Instrument Description and First Observations”, The Astronomical Society of the Pacific, 2007 February 16, Vol. 119, No. 852
7. https://www.prl.res.in/ shibu/mast/ao.html
8. C.U.Keller et al., “Low-cost solar adaptive optics in the infrared”, SPIE proceedings, Vol. 4853, 2003
9. R. Sridharan, “Techniques for achieving higher spatial resolution”, PhD thesis, Bangalore University, 2001
10. Goodman, “Fourier optics”, McGraw-Hill, 1996
11. Goodman, “Statistical optics”, Wiley, 2000
12. http://community.dur.ac.uk/james.osborn/thesis/thesisse3.html
13. http://cfao.ucolick.org/pubs/presentations/aosummer03/vanDam.pdf

14. R.Ramos et al, “The use of CPU, GPU and FPGA in real-time control of adaptive optics systems”, 2015

15. F.Roddier and C.Roddier, “Curvature sensing and compensation:a new concept in adaptive optics”, 1988

16. D.L.Fried, “Statistics of a geometrical representation of wavefront distortion”, Vol.55, No.11, Journal of Optical Society of America, 1965

17. W.H.Press et al., “Numerical Recipes”, 3rd Ed., Cambridge university press, 2007

18. Robert J.Noll, "Zernike polynomials and atmospheric turbulence", Nov.1975

19. D.L.Fried, "Statistics of a Geometric Representation of Wavefront Distortion", Feb.1965, Journal of the OSA, Vol.55, No.11

20. Guang-ming Dai, "Modal wave-front reconstruction with Zernike polynomials and Karhunen–Lo‘eve functions", 1996, Journal of the OSA, Vol.13, No.6

21. V.Mahajan, Zernike Polynomial Lecture "Introduction to aberrations", Apr 2012

22. Tyson, "Introduction to Adaptive Optics"

23. Chuong Bi.Do, "The Multi-Variate Gaussian Distribution", Oct 2008

24. M.Bahri et al., "Relation between Convolution and Correlation for Fourier Transform and Quaternion Fourier Transform", Int. Journal of Math Analysis, Vol.7, No.43, 2013

25. J.Wyant, K.Creath, "Basic Wavefront Aberration Theory for Optical Metrology", Applied Optics and Optical Engineering, Vol.11

26. Malacara, D., ed. “Optical Shop Testing.” Wiley, New York, (1978).